Vehicle Self-localization with High-Precision Digital Maps

Andreas Schindler

***Abstract*— Cooperative driver assistance functions benefit from sharing information on the local environments of individual road users by means of communication technology and advanced sensor data fusion methods. However, the consistent integration of environment models as well as the subsequent interpretation of traffic situations impose high requirements on the self-localization accuracy of vehicles. This paper presents methods and models for a map-based vehicle self-localization approach. Basically, information from the vehicular environment perception (using a monocular camera and laser scanner) is associated with data of a high-precision digital map in order to deduce the vehicle's position. Within the Monte-Carlo localization approach, the association of road markings is reduced to a prototype fitting problem which can be solved efficiently due to a map model based on smooth arc splines. Experiments on a rural road show that the localization approach reaches a global positioning accuracy in both lateral and longitudinal direction significantly below one meter and an orientation accuracy below one degree even at a speed up to 100 km/h in real-time.**

I. INTRODUCTION

In recent years, driver assistance systems contributed significantly to the reduction of traffic accidents and the mitigation of crash consequences. Wireless communication technologies as well as sensor data fusion methods across vehicles enable cooperative assistance functions. By sharing information on their local environments, the individual road users increase the robustness and completeness of knowledge on the surroundings and, thus, enrich the data basis for making decisions. Within the joint project Ko-PER, which is part of the research initiative Ko-FAS (cf. [1]), cooperative assistance functions are investigated in rural areas aiming to reduce crashes that occur at overtaking maneuvers, rear-end collisions or hazardous situations of crossing pedestrians. However, the consistent integration of environment models as well as the subsequent interpretation of traffic situations impose high requirements on the self-localization accuracy of vehicles. More precisely, a longitudinal and lateral position accuracy below $1\,\mathrm{m}$ and an orientation accuracy in the magnitude of 1° are required in order to distinguish between two adjacent vehicles and to associate road users and individual lanes. Hence, the vehicle self-localization represents an essential and challenging component for any cooperative system.

Since standard GNSS based localization techniques often cannot provide positioning results with the required accuracy and reliability defined above due to multi-path scattering, shading effects caused by the environment and atmospheric disturbances (cf. [2]), alternative and complementary global localization techniques must be considered.

Originating in the field of robot localization, simultaneous localization and mapping (SLAM) approaches are widely investigated (cf. [3] for a survey) in order to determine a vehicle's pose using a digital map created during driving. In the literature several vehicle self-localization approaches are known based on feature matching of laser scans like [4], [5], [6]. The work in [7] generates a feature map using aerial images. Road markings are detected based on stereo vision and characterized by their centroids, and the landmark association problem is realized by classical feature matching. In contrast, the approach in [8] uses texture interpretation to compare a texture feature map and image contents for a video-based self-localization in urban environments.

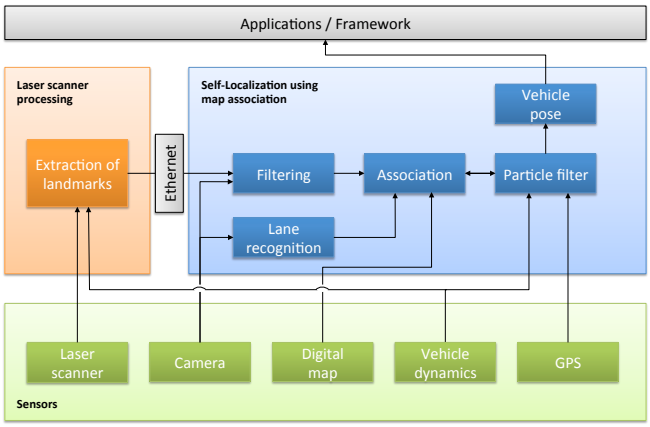

Fig. 1: Overview of the self-localization approach

This paper presents methods and models for a map-based vehicle self-localization approach. To begin with, Figure 1 shows an overview of the essential components. The basic idea is to associate information from the vehicular environment perception with the data of a high-precision digital map in order to deduce the vehicle's position and orientation.

Therefore, the involved environment perception methods based on a monocular gray value camera and a laser scanner are used to identify distinctive objects in the vehicle's surroundings. The sensor data processing allows detecting road markings using a video-based lane recognition system and extracting landmarks, like traffic signs, trees or guide posts, realized in a specific laser scanner processing unit. These extracted and reconstructed features are associated with elements in the digital map in order to correct the pose

Andreas Schindler is with FORWISS, the Institute for Software Systems in Technical Applications, University of Passau, 94032 Passau, Germany schindler@forwiss.uni-passau.de

estimation, which is roughly initialized with GPS. Intrinsic measurements of the vehicle dynamics, like the velocity and the turn rate, determine the motion model parameter of the vehicle.

Within the reference implementation, the probabilistic self-localization approach is realized using a Monte-Carlo Localization (MCL) technique (cf. [9]). Regarding the measurement update of the state estimation algorithm, the association with corresponding map elements is reduced to a prototype fitting problem.

II. DIGITAL MAP

The digital map model used for the present self-localization approach has been presented in [10]. Continuous road elements like individual lanes and road markings are represented by smooth arc splines, which are curves composed by smoothly joint circular arcs and line segments as depicted in Figure 2. This geometric model shows many advantageous properties regarding the efficient calculation of point to curve distances, best approximating points, offset curves and lengths of curve segments, which are calculations that are required in almost any map-based assistance function.

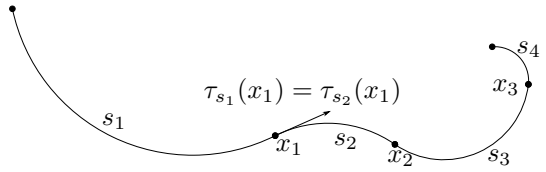

Fig. 2: Smooth arc spline with four segments $s_1, \ldots, s_4$ and breakpoints x_1, x_2, x_3. The equality of the tangent unit vectors $\tau_{s_1}(x_1)$ and $\tau_{s_2}(x_1)$ indicates the tangential smoothness at x_1.

Regarding the map generation, for any given maximal tolerance, the applied approximation method (cf. [11]) generates a smooth arc spline with a minimum number of segments. These properties are valuable for digital maps since they imply the checkability of accuracy of map elements as well as the minimization of the data volume required for storing the map. Furthermore, the mathematical particularities of arc splines are profitable not only for the self-localization observation models described in this work, but they represent an additional value for further automotive applications like the assignment of road users to lanes or for automated driving purposes.

Besides the representation of continuous road elements, the digital map contains individual landmarks of low lateral dimension, like traffic signs, guide posts or trees. Figure 3 shows a map section with elements that are relevant for the association process of the self-localization approach.

Within the project Ko-PER, a digital map of a rural area in the north of Munich has been created that includes the above mentioned map elements. The considered area offers a relatively high diversity regarding the natural environment (wood and grassland), the elevation profile (cambers and depressions) and, in particular, concerning the availability of road elements (road markings and landmarks). A total length of about $24\,\mathrm{km}$ of lanes has been mapped.

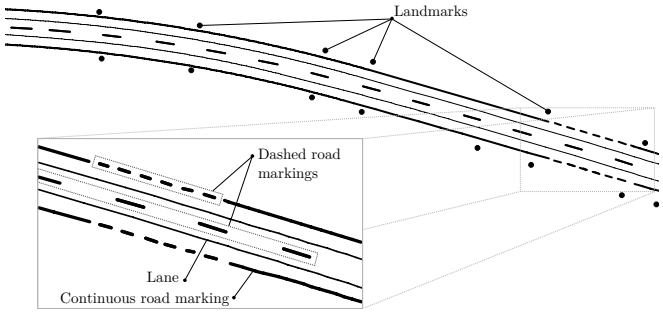

Fig. 3: Map section including lanes, road markings and landmarks.

By means of an independent evaluation by a third-party, the global accuracy of the map has been validated using high-precision reference points which were manually captured by a geodetic measuring system. Finally, the global root-mean-square error between the reference points and the road markings in the map has been measured to $0.1\mathrm{m}$ at randomly chosen evaluation points.

Regarding the localization approach, a fast access to map elements in a desired local environment around the vehicle is required. Within this context, index structures are suitable that represent a hierarchical decomposition of the digital map. For instance, a quadtree is a tree data structure where each node corresponds to a rectangular map section starting with the root which represents the whole digital map. If a node v is not a leaf then its four child nodes correspond to the quadrants of the map sections of v. Figure 4 shows a quadtree decomposition of a digital map section in the north of Munich up to the tree height 4. The zoom shows the map section of a leaf.

III. MAP-BASED SELF-LOCALIZATION

A. Environment perception

In the present case, the experimental vehicle is equipped with several sensors to perceive the local surroundings and to measure relevant vehicle parameters:

- The images of a monocular gray value camera are used in a lane recognition system similar to the one presented in [12]. For each frame, this method allows extracting a finite set of measurement points $P_{RM} \subset \mathbb{R}^2$ lying on road markings in the local environment of the vehicle.
- A processing unit for the scan data of a four layer laser scanner in the front of the vehicle provides hypotheses on landmarks in the surroundings.
- Intrinsic measurements on the velocity and the turn rate determine the motion model parameter of the vehicle.
- GPS is used for initialization and a rough estimation of the vehicle's pose.

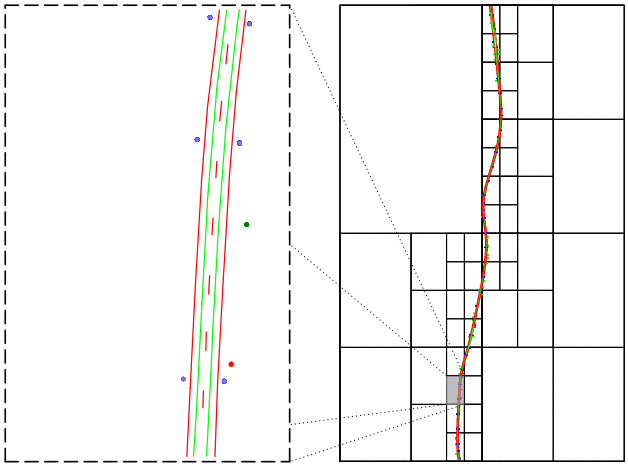

Fig. 4: Quadtree decomposition of a map section. Road markings are drawn in red while lanes are marked in green. Blue dots mark guide posts while the red and green dots represent a traffic sign and a tree.

B. Vehicle model and particle filtering

The internal state of the vehicle is modeled as a time-discrete Markov process with the parameters

$$\boldsymbol{x_k} = (x_k, y_k, \psi_k, v_k, c_k) \in \mathbb{R}^5 \tag{1}$$

at time $t_k \in \mathbb{R}, k \in \mathbb{N}$. The position (x_k, y_k) and the heading angle ψ_k form the pose of the vehicle within the navigation frame, which is comparable to the UTM coordinate system. The motion of the vehicle is described by the commonly known CTRV model, where it is assumed that the turn-rate and the velocity v_k is constant within small observation intervals. In this case, the vehicle moves on circular arc segments with curvature c_k, which allows predicting the vehicle's pose regarding the time.

In order to correct the pose estimation by incorporating measurements of the sensors, a sequential Monte-Carlo localization method is applied. As usual, the conditional state probability density is approximated empirically by a finite set of particles $x_k^{(i)}, 1 \leq i \leq M$ and corresponding weights $w_k^{(i)}$ at time t_k:

$$p(x|z_k, \ldots, z_0) \approx \sum_{i=1}^{M} w_k^{(i)} \delta(x - x_k^{(i)}) \tag{2}$$

for any sensor measurements $z_k, \ldots, z_0$ and the Dirac delta function δ. Regarding the weights, it is true that $w_k^{(i)} \geq 0$ and $\sum_{i=1}^{M} w_k^{(i)} = 1$. Each particle represents a state hypothesis whose weight is proportional to the conditional probability $p(z_k|x_k^{(i)})$ of observing the sensor measurement z_k given the state hypothesis $x_k^{(i)}$.

Assuming a normally distributed measurement noise process R_k, the likelihood for observing z_k given a state x_k can be expressed by

$$p(z_k|x_k) = p(R_k = (z_k - h(x_k))) \tag{3}$$

using an explicit observation model $h : \mathbb{R}^5 \to \mathbb{R}^m$ from the state space to the measuring space. While z_k denotes a *real sensor measurement*, the term $h(x_k)$ is called *predicted measurement* and the difference $z_k - h(x_k)$ is commonly named *residual* of the measurement update. Finally, the weights $w_k^{(i)}$ are given by

$$w_k^{(i)} = \frac{p(z_k \mid x_k^{(i)})}{\sum_{j=1}^{M} p(z_k \mid x_k^{(j)})}. \tag{4}$$

Since the sensor observations are available only at discrete points in time t_k, a SIR particle filter algorithm (see [13]) recursively updates the discrete approximation (2) in the following roughly summarized steps:

- *Prediction*: Each particle is predicted according to the vehicle motion model and the time difference to the next sensor measurement.
- *Filtering*: The weights of the particles are updated according to (4) using the sensor measurement.
- *Resampling*: The particles are redistributed within the state space based on their updated weights or according to a strategy based on a priori knowledge.

The individual points in time t_k are mainly determined by the acquisition time of the sensors. In the present case, for each measurement a precise time stamp is available which allows interpreting the observation temporally.

As usual within the context of particle filtering, no assumption on the type of the state probability density is made, which, in particular, allows multi-modality. This property can be exploited for modeling vehicle pose hypotheses on different lanes of the digital map by distributing particles explicitly on these lanes in the resampling step of the particle filter.

The final pose estimation required by the applications is extracted using Mean-Shift (cf. [14]) related clustering techniques based on the set of particles.

C. Observation models

With regard to equation (3), in the next sections it is focused on the definition of specific observation models and techniques for the association of map elements with measurements extracted by the vehicular environment perception.

1) Initialization: At the initialization phase of the localization system, the particles are normally distributed around a pose given by GPS with a covariance matrix determined by the uncertainty of the receiver. In the subsequent filter cycles, GPS is also used within the resampling step by setting the pose parameters of a small subset of particles to the GPS position.

2) Landmarks: Several approaches in the literature like [4], [15] deal with the association of laser scanner features with landmarks in a digital map for self-localization purposes. The more general data association problem with uncertainties regarding the correspondences can be treated with probabilistic methods like the *(Joint) Probabilistic Data Association* filter [16] which allows modeling concurrent association constellations between cluttered measurements

and landmarks in a statistical sense. Further examples for filter extensions are the *(Joint) Integrated Probabilistic Data Association* filter [17], which introduce a target existence propagation model. In the present case, a priori knowledge on the landmark association constellation is available based on the estimation of the vehicle's pose in the preceding frames, which can be used to reduce the combinatorial search space by means of gating techniques.

Since this landmark association problem is widely treated in the literature, we focus on the observation model of road markings in the following.

3) Road markings: In this paper, the association of road markings in the digital map with a set of measurement points extracted by the lane recognition is reduced to a prototype fitting problem: Introduced in [18] and continued in [19], the so-called *prototype fitting* is a generalization of the *iterated closest point* algorithm ([20]) regarding broader classes of admissible transformations and reference sets. For our purposes, the reference geometry is encoded as a compact subset $\Pi \subset \mathbb{R}^2$, e.g. as a union of curves, and it is called *prototype*. If points $y \in A \subset \mathbb{R}^2$ have been extracted within a measurement process, the *prototype fitting problem* is the challenge to find a feasible transformation $\Phi : \mathbb{R}^2 \to \mathbb{R}^2$ minimizing the sum of squares

$$\sum_{y \in A} \operatorname{dist}(\Phi(\Pi), y)^2, \tag{5}$$

where dist denotes the Euclidean distance. The question whether the prototype Π or the points A are transformed by Φ can be decided according to the computational effort. The solving strategy, described in the following, can be formulated for both decisions analogously. Within any prototype fitting problem, the determination of best approximating points $x_y \in \Pi$ for each $y \in A$ is the bottleneck of the computing time. Therefore, a suitable encoding of Π, which minimizes the computational requirements for the best approximating point calculation, is essential.

Naturally, the existence of optimal motions can only be assured if some restrictions and assumptions on the feasible transformations are made. In the present case, the admissible transformations are restricted to rotations and translations, which are mappings of the form

$$T_{\varphi,t} : \mathbb{R}^2 \to \mathbb{R}^2, \quad x \mapsto \begin{pmatrix} \cos(\varphi) & -\sin(\varphi) \\ \sin(\varphi) & \cos(\varphi) \end{pmatrix} \cdot x + t, \tag{6}$$

with $\varphi \in [0, 2\pi[$ and $t \in \mathbb{R}^2$. Hence, optimal parameters $\varphi \in [0, 2\pi[$ and $t \in \mathbb{R}^2$ are searched within the prototype fitting problem. In this case the problem can be solved by an iterative approach.

To begin with, it is assumed that some initial transformation parameter φ_0, t_0 are known such that the transformed prototype Π approximately fits to the points A. Starting with $\Pi^{(0)} := \Pi$, in the j-th step for $j \in \mathbb{N}$, the best approximating points $x_i^{(j)}$ of y_i with respect to the set

$$\Pi^{(j)} := T_{\varphi_{j-1}, t_{j-1}}(\Pi^{(j-1)}) \tag{7}$$

are computed. Using the abbreviation

$$\widetilde{x}_i^{(j)} := \begin{pmatrix} 0 & -1 \\ 1 & 0 \end{pmatrix} x_i^{(j)} \text{ for all } i = 1, \ldots, n \tag{8}$$

and denoting the barycenters of $x_1^{(j)}, \ldots, x_n^{(j)}$ and $y_1, \ldots, y_n$ by

$$\mu_{x^{(j)}} := \frac{1}{n} \sum_{i=1}^{n} x_i^{(j)} \text{ and } \mu_y := \frac{1}{n} \sum_{i=1}^{n} y_i, \tag{9}$$

the optimal values $\varphi_j \in [0, 2\pi[$ and $t_j \in \mathbb{R}^2$, i.e.

$$\sum_{i=1}^{n} \left\| T_{\varphi_j, t_j}(x_i^{(j)}) - y_i \right\|^2 = \min_{\substack{\varphi \in [0, 2\pi[\\ t \in \mathbb{R}^2}} \sum_{i=1}^{n} \left\| T_{\varphi, t}(x_i^{(j)}) - y_i \right\|^2 \tag{10}$$

can be derived in a closed form: Using $c_j, s_j \in \mathbb{R}$ with

$$c_j = \frac{1}{\rho} \sum_{i=1}^{n} (x_i^{(j)} - \mu_{x^{(j)}})^T y_i, \;\; s_j = \frac{1}{\rho} \sum_{i=1}^{n} (\widetilde{x}_i^{(j)} - \mu_{x^{(j)}})^T y_i, \tag{11}$$

where $\rho = \sum_{i=1}^{n} \left\| x_i^{(j)} - \mu_{x^{(j)}} \right\|^2$, the optimal rotation angle is given by

$$\varphi_j = \arccos\left(\frac{c_j}{\sqrt{c_j^2 + s_j^2}} \right) \tag{12}$$

and the optimal translation is given by $t_j = \mu_y - A_{\varphi_j} \mu_{x^{(j)}}$. Using the abbreviation $T_j := T_{\varphi_j, t_j}$, the value

$$E_j := \frac{1}{n} \sum_{i=1}^{n} \left\| T_j(x_i^{(j)}) - y_i \right\|^2 \tag{13}$$

indicates the prototype fitting error at step j. One can show that the sequence $(E_j)_{j \in \mathbb{N}}$ is monotonic decreasing. By increasing j, the best approximating points $x_i^{(j+1)}$ of y_i with respect to $\Pi^{(j+1)}$ can be computed and the least squares problem is solved iteratively. This alternating procedure is continued while E_j is greater than some given threshold or the difference between the predecessor error and the current error is not smaller than some given threshold.

Coming back to the self-localization problem, the prototype Π consists of all road markings in a local environment of the vehicle, the fitting points are the measurement point s P_{RM} extracted by the lane recognition from Section III-A and the initial transformation is based on the pose parameter (x_k, y_k, ψ_k) of the current vehicle state.

As already discovered in [20] and [18], the necessity of a fast determination of best approximating points does not depend on a special choice of the optimization method but it is also crucial when using any other nonlinear optimization algorithm, like Gauß-Newton or Levenberg-Marquardt.

Indeed, the efficiency of distance calculations depends on the encoding of the prototype Π. Therefore, a description of Π as a union of curves having a preferably low number of segments and providing a fast calculation of best approximating points is preferable. Since the geometric model of road markings in the digital map is based on arc splines, these calculations are highly efficient due to two reasons:

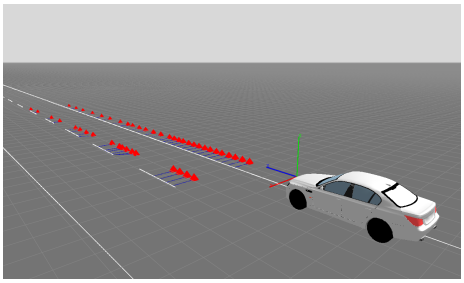

Fig. 5: Association of measurement points P_{RM} (red pyramids) with road markings for the pose correction based on prototype fitting.

The calculation of best approximating points on arc spline segments can be realized in a simple closed form which, in general, is not the case for many other curve types like polynomial splines of degree > 2 or clothoids. Furthermore, the minimality of the segment number guaranteed by the arc spline approximation ensures that the road markings are encoded in a compact way and thus reduce the search space of segments for best approximating points.

Regarding the filtering methodology in (3), the fitting points $P_{RM} = y_1, \ldots, y_n$ represent some real measurements of a measurement update at time t_k. Their corresponding predicted measurements are given by the best approximating points with respect to the prototype Π transformed by the initial transformation T_0. Therefore, the road marking observation model can be expressed as a family of functions $(h_i)_{i=1,\ldots,n} : \mathbb{R}^5 \to \mathbb{R}^2$ for any state $\boldsymbol{x}_k \in \mathbb{R}^5$ at time t_k:

$$h_i(\boldsymbol{x}_k) = \underset{p \in T_0(\Pi)}{\operatorname{argmin}} \operatorname{dist}(y_i, p) \tag{14}$$

where dist denotes the Euclidean distance. Thus, the residual vector

$$v_k := \begin{pmatrix} y_1 - h_1(\boldsymbol{x}_k) \\ \vdots \\ y_n - h_n(\boldsymbol{x}_k) \end{pmatrix} \tag{15}$$

is related to the prototype fitting error since

$$\frac{1}{n} \sum_{i=1}^{n} \left\| x_i^{(1)} - y_i \right\|^2 = \frac{1}{n} \left\| v_k \right\|^2 \tag{16}$$

for the best approximating points $x_i^{(1)}$ of y_i with respect to the transformed prototype $T_0(\Pi)$.

Beside the presented observation model, a resampling strategy for particles can be applied using the same principle: Since the prototype fitting determines a transformation that best fits Π onto P_{RM} in the least-squares sense above, it can be used to correct the pose estimation represented in each particle $x_k^{(i)}$ at time t_k in a direct way. Therefore, let $n \in \mathbb{N}$ denote the number of applied fitting steps leading to the final transformation $T^\star := T_n \circ \cdots \circ T_0$. Related to the classical map-matching principle, one can show that applying the inverse mapping of $T^\star$ to the pose parameters (x_k, y_k, ψ_k) of a particle improves the pose estimation with respect to the prototype fitting error defined in (13).

IV. RESULTS

In order to evaluate the performance of the proposed self-localization approach, a RTK-GPS reference positioning system is used, which fuses differential GPS with high-precision inertial measurements. Under good conditions, a global localization accuracy of $0.02\,\mathrm{m}$ is reached with this reference system, making it suitable for evaluation purposes.

The self-localization approach is tested in different scenarios regarding the level of map details (availability of landmarks and road markings), weather conditions, sensor configurations and driving maneuver on the rural road section in Ko-PER. The localization results are compared to the high-precision reference system, where the positional error plots refer to the lateral and longitudinal orientation of the vehicle. Additionally, the mean value and standard deviation of the absolute errors are indicated below the figures. It should be noted that all errors refer to global positioning results and not to relative errors regarding the map. Figure 6a and 6b show the lateral and longitudinal localization error on a road section of about $4\,\mathrm{km}$. One can see that the global localization error is significantly below $1\,\mathrm{m}$ for both directions. The red shaded areas in the plots represent the uncertainty of the RTK-GPS reference. The remaining error peaks can be traced back either to outliers in the reconstruction of measurements within the environment perception, to errors in the digital map concerning the accuracy of map elements or to wrong associations of measurement points with map objects. The systematic longitudinal localization error of about $0.4\,\mathrm{m}$ is probably due to a suboptimal assignment of timestamps to a laser scan since this kind of localization error could be observed for both driving directions of the road section.

Figure 6c shows that the global heading error is significantly below $1°$. Furthermore, Figure 6d and Figure 6e depict the driven velocity and the availability of landmarks per system frame corresponding to an interval of $0.08\,\mathrm{s}$ ($12.5\,\mathrm{Hz}$).

Within the reference implementation of the self-localization approach, the processing time for one frame is below $0.01\,\mathrm{s}$ on a $2.8\,\mathrm{GHz}$ CPU which makes the system fully real-time capable.

An extensive evaluation and more details on the presented approach will be available in [21].

V. SUMMARY

In this paper some aspects of a map-based vehicle self-localization approach have been presented. Environment perception methods are used to detect and associate relevant objects with corresponding elements in a high-precision digital map. Continuous map elements are modeled as smooth arc splines which show advantageous properties like the efficient distance calculation. The presented observation model based on prototype fitting benefits from these particularities and forms a suitable component of the probabilistic localization strategy using particle filtering. Experiments show that a global localization error below $1\,\mathrm{m}$ and an orientation error below $1°$ can be reached with the presented methods.

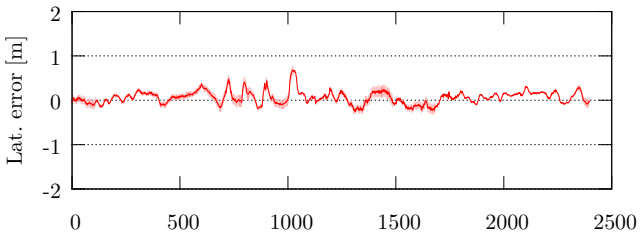

(a) $e_{lat} = 0.120\,\mathrm{m} \quad \sigma_{e_{lat}} = 0.096\,\mathrm{m}$

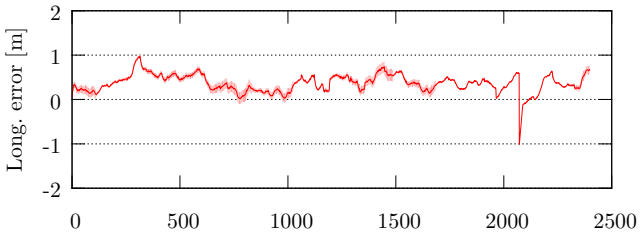

(b) $e_{lon} = 0.371\,\mathrm{m} \quad \sigma_{e_{lon}} = 0.178\,\mathrm{m}$

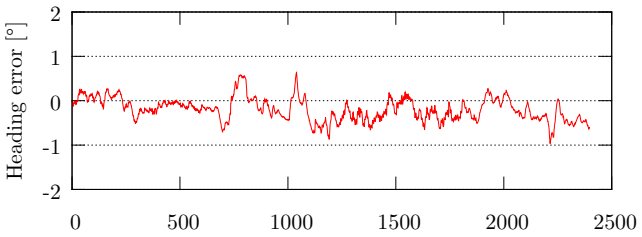

(c) $e_{\psi} = 0.266° \quad \sigma_{e_{\psi}} = 0.185°$

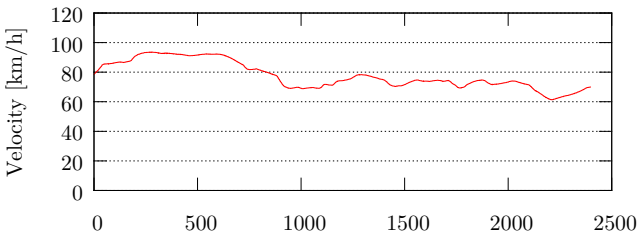

(d) Average velocity: 77.6 km/h

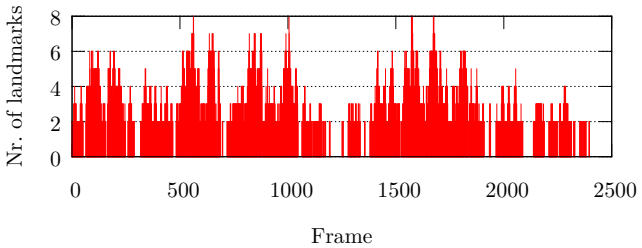

(e) Average number of landmarks per frame: 2.69

Fig. 6: Localization results in a data sequence of a rural road section. The horizontal time axes is quantified in frames (1 Frame = 0.08 s).

ACKNOWLEDGMENT

This work results from the joint project Ko-PER, which is part of the project initiative Ko-FAS, and has been funded by the German Bundesministerium für Wirtschaft und Technologie (Federal Department of Commerce and Technology) under grant number 19 S 9022E.

We would like to thank BMW Group Research and Technology (by name A. Rauch, K. Vogel and F. Klanner) and SICK AG (by name R. Krzikalla) for the cooperation in this project and for providing the vehicular platform and sensor data of various test scenarios.

REFERENCES

[1] "Ko-FAS," http://www.ko-fas.de.

[2] *Global Positioning System Standard Positioning Service Performance Standard*. Department of Defense USA & GPS NAVSTAR, 2008.

[3] S. Thrun, "Robotic Mapping: A Survey," in *Exploring Artificial Intelligence in the New Millenium*, G. Lakemeyer and B. Nebel, Eds. Morgan Kaufmann, 2002.

[4] T. Weiss, N. Kaempchen, and K. Dietmayer, "Precise ego-localization in urban areas using Laserscanner and high accuracy feature maps," in *Proc. of the IEEE Intelligent Vehicles Symposium*, 2005, pp. 284–289.

[5] R. Schubert, N. Mattern, M. Schlingelhof, F. Ahlers, and D. Westhoff, "Vehicle positioning for cooperative systems - the SAFESPOT approach," in *Proc. of the 16th World Congress on Intelligent Transportation Systems*, 2009.

[6] F. Ahlers and D. Westhoff, "Precise Laserscanner-based positioning on intra-urban crossings," in *SAFESPOT Technical presentations to the 16th World Congress on Intelligent Transportation Systems*, 2009.

[7] O. Pink and C. Stiller, "Automated map generation from aerial images for precise vehicle localization," in *Proc. of the IEEE Conference on Intelligent Transportation Systems*, 2010, pp. 1517–1522.

[8] N. Mattern and G. Wanielik, "Camera-based Vehicle Localization at Intersections using Detailed Digital Maps," in *Position Location and Navigation Symposium*, 2010.

[9] S. Thrun, D. Fox, W. Burgard, and F. Dellaert, "Robust Monte Carlo Localization for Mobile Robots," *Artificial Intelligence*, vol. 128, no. 1-2, pp. 99–141, 2000.

[10] A. Schindler, G. Maier, and F. Janda, "Generation of high precision digital maps using circular arc splines," in *Proc. of the IEEE Intelligent Vehicles Symposium*, 2012, pp. 246–251.

[11] G. Maier, *Smooth Minimum Arc Paths. Contour Approximation with Smooth Arc Splines*. Shaker, 2010.

[12] T. Tatschke and J. Urlhardt, "Model-based road lane extraction from monocular image sequences," *PReVENT Fusion Forum eJournal Vol. 2*, 2008.

[13] M. Arulampalam, S. Maskell, N. Gordon, and T. Clapp, "A tutorial on particle filters for online nonlinear/non-Gaussian Bayesian tracking," *IEEE Transactions on Signal Processing*, vol. 50, no. 2, pp. 174–188, 2002.

[14] Y. Cheng, "Mean Shift, Mode Seeking, and Clustering." *IEEE Trans. Pattern Anal. Mach. Intell.*, vol. 17, no. 8, pp. 790–799, 1995.

[15] F. Lu and E. E. Milios, "Robot Pose Estimation in Unknown Environments by Matching 2D Range Scans." *Journal of Intelligent and Robotic Systems*, vol. 18, no. 3, pp. 249–275, 1997.

[16] Y. Bar-Shalom, F. Daum, and J. Huang, "The probabilistic data association filter," *Control Systems*, vol. 29, no. 6, pp. 82–100, 2009.

[17] D. Musicki and R. Evans, "Joint Integrated Probabilistic Data Association - JIPDA," in *Proc. of the Fifth International Conference on Information Fusion*, vol. 2, 2002, pp. 1120–1125.

[18] K. Donner, "Image Interpretation Based on Local Transform Characterization," *Pattern Rec. and Image Analysis*, vol. 7, no. 4, 1997.

[19] G. Maier and A. Schindler, "Visual Quality Control of Planar Working Pieces: A Curve Based Approach Using Prototype Fitting." in *ICCSA (4)*, ser. Lecture Notes in Computer Science, vol. 6785. Springer, 2011, pp. 91–102.

[20] P. J. Besl and H. D. McKay, "A method for registration of 3-D shapes," *IEEE Transactions on Pattern Analysis and Machine Intelligence*, vol. 14, no. 2, pp. 239–256, Feb. 1992.

[21] A. Schindler, "Vehicle Self-Localization Using High-Precision Digital Maps," Ph.D. dissertation, Universität Passau, to be published in 2013.